# Phototransduction by Vertebrate Ultraviolet Visual Pigments: Protonation of the Retinylidene Schiff Base following Photobleaching†

Abhiram Dukkipati,[‡,§,||,⊥] Anakarin Kusnetzow,[‡,⊥,#] Kunnel R. Babu,[§] Lavoisier Ramos,[‡,▽] Deepak Singh,[‡,▼] Barry E. Knox,*[,§] and Robert R. Birge*[,‡,▽]

*Departments of Chemistry and Biology, Syracuse University, 111 College Place, Syracuse, New York 13244-4100, Department of Biochemistry and Molecular Biology, SUNY Upstate Medical University, 750 East Adams Street, Syracuse, New York 13210, and Department of Chemistry, University of Connecticut, Storrs, Connecticut 06269*

*Received March 27, 2002; Revised Manuscript Received May 29, 2002*

ABSTRACT: The photochemical and subsequent thermal reactions of the mouse short-wavelength visual pigment (MUV) were studied by using cryogenic UV−visible and FTIR difference spectroscopy. Upon illumination at 75 K, MUV forms a *batho* intermediate ($\lambda_{max}$ ~380 nm). The *batho* intermediate thermally decays to the *lumi* intermediate ($\lambda_{max}$ ~440 nm) via a slightly blue-shifted intermediate not observed in other photobleaching pathways, *BL* ($\lambda_{max}$ ~375 nm), at temperatures greater than 180 K. The *lumi* intermediate has a significantly red-shifted absorption maximum at 440 nm, suggesting that the retinylidene Schiff base in this intermediate is protonated. The *lumi* intermediate decays to an even more red-shifted *meta I* intermediate ($\lambda_{max}$ ~480 nm) which in turn decays to *meta II* ($\lambda_{max}$ ~380 nm) at 248 K and above. Differential FTIR analysis of the 1100−1500 $cm^{-1}$ region reveals an integral absorptivity that is more than 3 times smaller than observed in rhodopsin and VCOP. These results are consistent with an unprotonated Schiff base chromophore. We conclude that the MUV−visual pigment possesses an unprotonated retinylidene Schiff base in the dark state, and undergoes a protonation event during the photobleaching cascade.

SWS1[1] pigments mediate visual sensitivity in the short-wavelength region of the spectrum, exhibiting absorption maxima ($\lambda_{max}$) between 350 and 450 nm, the widest energy range in the opsin classes (*1*). Moreover, SWS1 pigments are the only opsins with absorption maxima blue-shifted compared to a protonated retinylidene Schiff base in aqueous solution, $\lambda_{max}$ = 440 nm (*2*). The pigments in the SWS1 group are divided into two subgroups based on the absorption maxima: those that absorb in the 400−440 nm range (blue/violet) and those that absorb in the 350−390 nm range (UV). One explanation for the variation in $\lambda_{max}$ hypothesizes that SWS1 pigments with $\lambda_{max}$ in the UV (<400 nm) have an unprotonated Schiff base while those with $\lambda_{max}$ in the blue−violet region ($\lambda_{max}$ >400 nm) have a protonated Schiff base (*3*). However, the molecular mechanisms of spectral tuning in SWS1 pigments may also include contributions from the relative position of the counterion to the Schiff base, and multiple dispersive interactions distributed among numerous amino acids in the retinal binding pocket (*4*).

Studies on the phototransduction properties of *Xenopus* (*5*), human (*6*), and salamander (*7*) SWS1 pigments have shown reduced catalytic efficiency and shorter lifetime of the light-activated conformation compared to bovine rhodopsin. These differences in signal transduction may play an important role in shaping the dynamics of light response in cones (*8*, *9*). To understand the molecular basis for the unique functional properties of SWS1 pigments, detailed spectroscopic, biochemical, and site-directed mutagenesis studies are required, in pigments that absorb both in the UV as well as in the violet region.

We have previously studied spectral tuning and phototransduction in the *Xenopus* SWS1 opsin (VCOP, $\lambda_{max}$ ~427 nm). FTIR difference spectroscopy used to examine the *meta II* intermediate (*10*) and site-directed mutagenesis studies (*11*) have shown that the retinylidene Schiff base linkage is protonated in the dark state. Furthermore, the counterion (D108) to the protonated Schiff base was found to be at the

† This work was supported in part by NIH Grants GM-34548 (to R.R.B.) and EY-11256 and EY-12975 (to B.E.K.), the W. M. Keck Center for Molecular Electronics at Syracuse University, and a grant from the Research to Prevent Blindness Foundation.

* Correspondence should be addressed to either B.E.K.: tel (315) 464-8719, fax (315) 464-8750, email knoxb@upstate.edu; or R.R.B.: tel (860) 486-6720, fax (860) 486-2981, email: rbirge@uconn.edu.

‡ Syracuse University.

§ SUNY Upstate Medical University.

|| Present address: Department of Microbiology and Immunology, 299 Campus Dr., Stanford School of Medicine, Stanford, CA 94305.

⊥ These authors contributed equally to this work.

# Present address: Jules Stein Eye Institute, UCLA School of Medicine, 100 Stein Plaza, BH-973, Los Angeles, CA 90095.

▽ University of Connecticut.

▼ Present address: GeneFormatics Inc., 5830 Oberlin Dr., Suite 200, San Diego, CA 92121.

[1] Abbreviations: SWS1, short-wavelength-sensitive; MUV, mouse SWS1 opsin; VCOP, *Xenopus laevis* SWS1 opsin; RH, rhodopsin(s); M/LWS, medium/long-wavelength-sensitive; TM#, transmembrane helical domain #; SB, Schiff base; nm, nanometers; PSS(*xyz*), photostationary state generated by illumination at wavelength *xyz* in nanometers; DM, *n*-dodecyl-β-D-maltoside; HEPES, *N*-(2-hydroxyethyl)piperazine-*N*′-2-ethanesulfonic acid; *batho*, *lumi*, *meta I*, and *meta II*, discrete thermal intermediates of the visual opsin bleaching pathway; *BL*, photobleaching intermediate formed between *batho* and *lumi*; PSS, photostationary state.

10.1021/bi025883g CCC: $22.00 
Published on Web 07/11/2002

same position in TM3 as in bovine rhodopsin (*11*). During photobleaching, VCOP undergoes four spectrally discrete conformational changes analogous to the intermediates state described for rhodopsin: *batho*, *lumi*, *meta I*, and *meta II* (*10*). We have also suggested that the counterion and residues that interact with the counterion (e.g., S85 in TM2) play an important role in regulating the photobleaching pathway and ability to activate transducin (*4, 11*). These studies have led us to propose the extended counterion model for the SWS1 pigments (*4*).

Although the mouse SWS1 (MUV) contains 11-*cis*-retinal covalently attached via a Schiff base linkage to the protein (*11, 12*), the $\lambda_{max}$ ~357 nm suggests the Schiff base is unprotonated. The strongest supporting evidence comes from a site-specific mutant at the putative counterion position, E108Q (*11, 13*). Unlike bovine rhodopsin, in which the mutation of the counterion (E113Q) causes a dramatic change in the Schiff base p$K_a$ and an accompanying shift in the $\lambda_{max}$ to 380 nm at neutral pH (*14*−*16*), no significant change was observed in the MUV counterion mutant (*11, 13*).

In rhodopsin, Schiff base deprotonation accompanies the formation of *meta II*, the active intermediate state (*17, 18*). Site-specific mutants (e.g., E113Q, G90D, H211C) that alter the p$K_a$ of the Schiff base, either in the dark or after isomerization of the chromophore, dramatically affect the photobleaching properties of rhodopsin (*14, 19, 20*). E113, the counterion, is the acceptor of the Schiff base proton, and mutation of the counterion to a neutral residue slows the decay of the later photointermediates (*21*). Similar disturbances in the photobleaching pathway of VCOP, which also contains a protonated Schiff base, were observed in counterion mutants (*11*). In addition, previous data reported from cryogenic experiments are consistent with an unprotonated Schiff base (*3*). If the UV-sensitive SWS1 pigments have an unprotonated Schiff base in the dark, does a protonation event occur upon light activation, and, if so, what is the role of the protonation of the Schiff base in phototransduction of these pigments?

To address this question, we have carried out a detailed spectroscopic and biochemical study of MUV, characterizing the complete photobleaching pathway of this pigment. We observe the formation of a *batho* intermediate, indicating normal *cis* to *trans* isomerization, as well as the formation of the later intermediates, *lumi*, *meta I*, and *meta II*. Most significantly, the Schiff base undergoes a protonation following photobleaching, most likely during the transition from *batho* to *lumi*.

## MATERIALS AND METHODS

*Expression, Isolation, and Purification of the Visual Pigments*. The MUV pigments contained the first 328 codons of the MUV coding region followed by the last 14 codons of bovine rhodopsin as an epitope tag (*3*). Transfection into COS1 cells and preparation of MUV pigments were performed as previously described (*3, 10, 11*). Typically, thirty 150 mm plates were transfected. The pigment was purified and concentrated to ~300 $\mu$L. MUV samples had an average $A_{360}$ between 0.3 and 0.4, with an $A_{280}/A_{360}$ of ~4.0. All pigments were stored in the dark at −80 °C. Experiments were repeated with pigment purified from at least two separate transfections.

*Cryogenic Electronic Spectroscopy*. Low-temperature spectroscopy was performed as previously described (*3, 10*). Samples for cryogenic studies were prepared in 67% glycerol, 0.05% *n*-dodecyl-$\beta$-D-maltoside (DM, Anatrace, Maumee, OH) in buffer A (buffer A = 50 mM HEPES, 140 mM NaCl, 3 mM $MgCl_2$, pH 6.6) with a final $A_{360} \sim 0.1$. Samples for cryogenic studies at 45−200 K were placed in an Air Products Displex helium-refrigerated cryostat coupled to a Shimadzu 3010 UV−vis−NIR spectrophotometer as described previously (*3, 10*). Samples for studies at 240−273 K were placed in a Varian Cary 3E modified for accurate temperature control as described previously (*10*). The photostationary states (PSS) were generated by successive illuminations at 305 nm until no further spectral changes could be detected (~1 h, unless specified otherwise).

The spectra shown in the figures are the averages of four separate scans at each temperature. The $\lambda_{max}$ absorbance values of the initial dark sample were used to normalize the spectra from different experiments. Each of the difference spectra was calculated by subtracting the appropriate photostationary state from the corresponding dark or previous photostationary state using SigmaPlot (Jandel, Chicago, IL).

*FTIR Difference Spectroscopy*. Glycerol and HEPES were removed from the protein sample (*10*). The buffer of the sample was changed to buffer B [10 mM potassium phosphate buffer (pH 6.8) and 0.02% DM], using Centricon C-30 filters, and excess peptide (1D4) in the sample was also removed using prepacked Sephadex G-50 columns (Pharmacia, Piscataway, NJ) (*10*). The sample was reconcentrated to ~100 $\mu$L. A thin film of the protein (~100 $\mu$g in 100 $\mu$L) was prepared by drying the sample in 10 $\mu$L aliquots onto a cool $CaF_2$ IR window under a continuous stream of nitrogen. This was repeated until successive layers were formed. The film was sealed with another $CaF_2$ window. The window was mounted on a Nicolet Magna IR 750, series II, instrument (Nicolet Instrument Corp., Madison, WI). The sample was kept equilibrated at 263 K for 1 h. The dark-state spectra were taken by averaging 512 scans at 2 $cm^{-1}$ resolution. To generate *meta II*, the sample was generated by illumination with light from a filtered (305 nm cutoff filter, Melles Griot 03FCG121) 250 W quartz halogen lamp (illumination time = 5 min) at 263 K. The sample was again illuminated for an additional 5 min to guarantee complete formation of the *meta II* state, and spectra were collected. Data collection was performed using OMNIC 3.1 (Nicolet Instrument Corp). The amide I peak (1654 $cm^{-1}$) of the dark-state and *meta II* state spectra was normalized. The dark-state spectrum was subtracted from the *meta II* state spectrum to generate the difference spectrum. The resulting difference spectrum of the second illumination was the same as with the first illumination, indicating complete formation of the photoproduct at 263 K.

*HPLC Analysis*. After illumination, visual pigment samples were warmed to 0 °C, and hydroxylamine was added to a final concentration of 500 mM, pH 7. Retinal oximes of the PSS305 generated at 243 K were extracted and analyzed as previously reported (*3*), and these values were used for all subsequent analysis.

*Homology Models*. The crystal structure of bovine rhodopsin, PDB accession no. 1F88 (*22*), was used to construct homology models for VCOP and MUV. The sequence of bovine rhodopsin was aligned with the sequences for VCOP

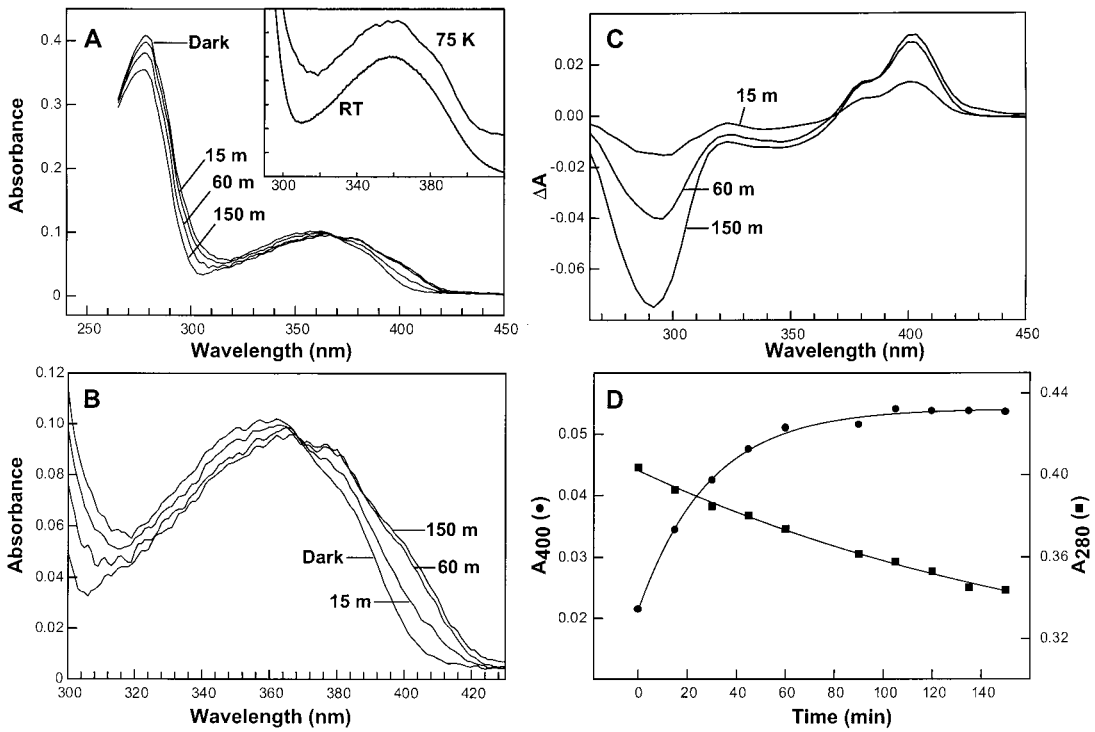


FIGURE 1: Photochemistry of the mouse SWS1 at cryogenic temperatures. Mouse SWS1 opsin (dark) was illuminated at 75 K with 305 nm light to generate the primary PSS305. (A and B) Spectra after successively illuminating the dark state (in minutes). The inset in panel A shows the spectra of MUV at room temperature (RT) and at 75 K. (C) Light − dark difference spectra generated by subtracting the dark state from the PSS305 after 15, 60, and 150 min of illumination. (D) Plot of the absorbance changes monitored at 280 and 400 nm during the successive illuminations. Lines are single-exponential fits to the data.

and MUV using CLUSTALW (*23*). These alignments were used to construct models for VCOP and MUV using the program WHATIF (*24*). Hydrogens were added in CHARMM (version 27b2) (*25*). The models were minimized by 4000 steps of the adopted-basis Newton Raphson (ABNR) algorithm using the charmm22 force field (*26*). The environment was represented by a distant-dependence (1/*r*) dielectric function. The initial chromophore geometry was retained from the X-ray structure. The retinylidene chromophore was represented by a potential adapted from the CHARMM-optimized all-*trans*-retinyl-protonated Schiff base (*27*). All calculations were performed with harmonic constraints on the protein backbone.

## RESULTS

*Formation of the Early Intermediates.* Improvements in the yield of MUV from transfected COS1 cells (*11*) have permitted cryogenic studies of this pigment at higher concentrations than in our previous reports, eliminating the light-scattering component and permitting an analysis of the low-temperature intermediates without correction of the spectra. Upon cooling to 75 K, the MUV spectrum undergoes a small 2 nm red shift ($\lambda_{max}$ ~359 nm, Figure 1A, inset) and exhibits a shoulder at ~380 nm. Illumination of the dark sample at 305 nm caused a red shift in the chromophore peak, which was complete within 1 h of illumination (Figure 1B,D). There also was a decrease in the protein extinction coefficient that accompanied the batho shift in the chromophore peak, and continued to decrease after the chromophore peak had reached a stationary state (Figure 1C, also see below). This photostationary state (PSS305) consisted mainly of the *batho* intermediate (all-*trans*-retinal bound to opsin) and a minor component of the original (11-*cis*-retinal bound to opsin) dark state (11-*cis*-retinal bound to opsin). There was very little isopigment (9-*cis*-retinal) formed under these conditions. The isomeric composition of the PSS305 generated at higher temperatures (243 K) had 11% 11-cis, 83% all-trans, and 5% 9-cis, ±2%.

The difference spectrum between PSS305 and the dark state has an absorption maximum at 404 nm and exhibits vibronic fine structure at $\lambda_{max}$ ~380 nm (Figure 1C), consistent with our earlier report (*3*). Thus, MUV forms a red-shifted primary photoproduct like another SWS1 pigment, VCOP (which has a protonated Schiff base linkage), and other visual pigments (*3*, *28*).

To trap the additional intermediates in the bleaching pathway, the batho-shifted PSS305 was gradually warmed from 80 to 220 K. After equilibrating the sample at a specified temperature (i.e., 180 K), the sample was gradually cooled back to 75 K where all spectra were collected to avoid artifacts arising from temperature-dependent baseline shifts. Small changes in the absorption spectrum of PSS305 between 120 and 180 K were observed (Figure 2A), primarily a decrease in the fine structure at 380 nm. Multiple changes in the absorption spectrum occurred at temperatures above 180 K: an increase in absorbance at wavelengths from 420 to 540 nm, a decrease in absorption of the 404 nm component, and an increase in absorbance at 280 nm (Figure 2). These changes are consistent with the thermal transition to another intermediate in the photobleaching pathway, presumably *lumi*. However, the absence of a clear isosbestic point during the *batho* to *lumi* transition suggests the presence of an additional intermediate during the transition, whose absorption spectrum overlaps significantly with the *batho*

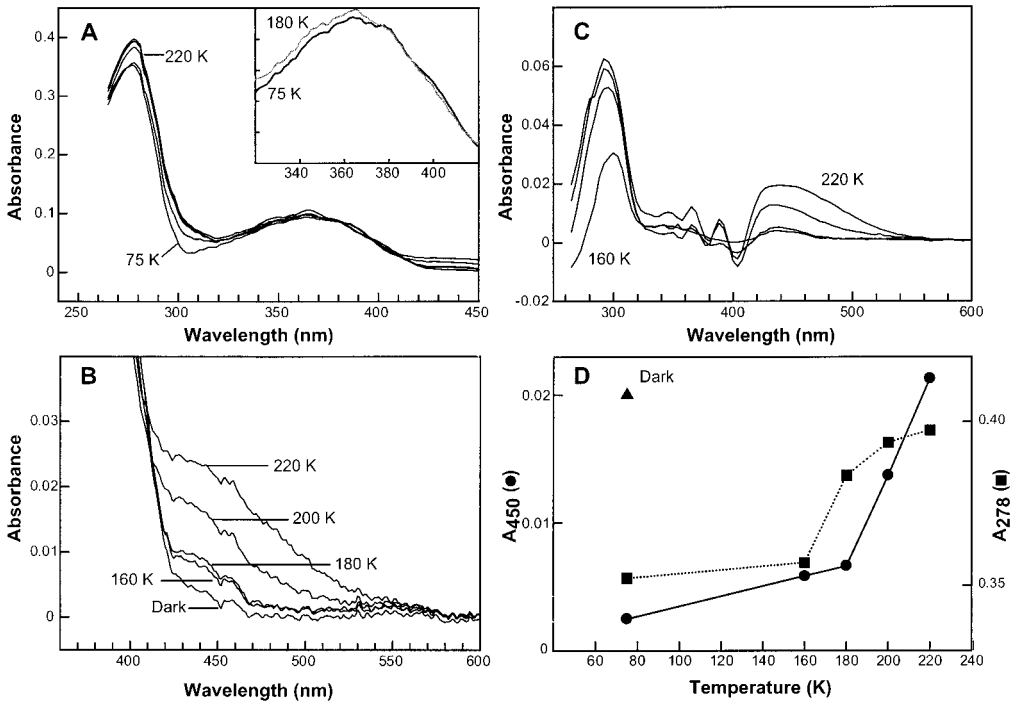


FIGURE 2: Thermal decay of the mouse SWS1 photostationary state formed at 75 K. The PSS305 formed at 75 K (spectrum labeled 75 K) was gradually warmed in 20 K increments, equilibrated for 1 h, and cooled back to 75 K before recording the absorption spectra. (A and B) Spectra of PSS305 after equilibration at 75, 160, 180, 200, and 220 K, respectively. The inset in (A) shows, on an expanded scale, only a minor change in the main chromophore peak in the sample warmed to 180 K compared to the initial PSS305 at 75 K. (C) Light − dark difference spectra generated by subtracting the dark state at 75 K from the PSS305 warmed to 160, 180, 200, and 220 K, respectively. (D) Plot of the absorbance changes monitored at 280 and 450 nm during the temperature ramping experiments in (A).

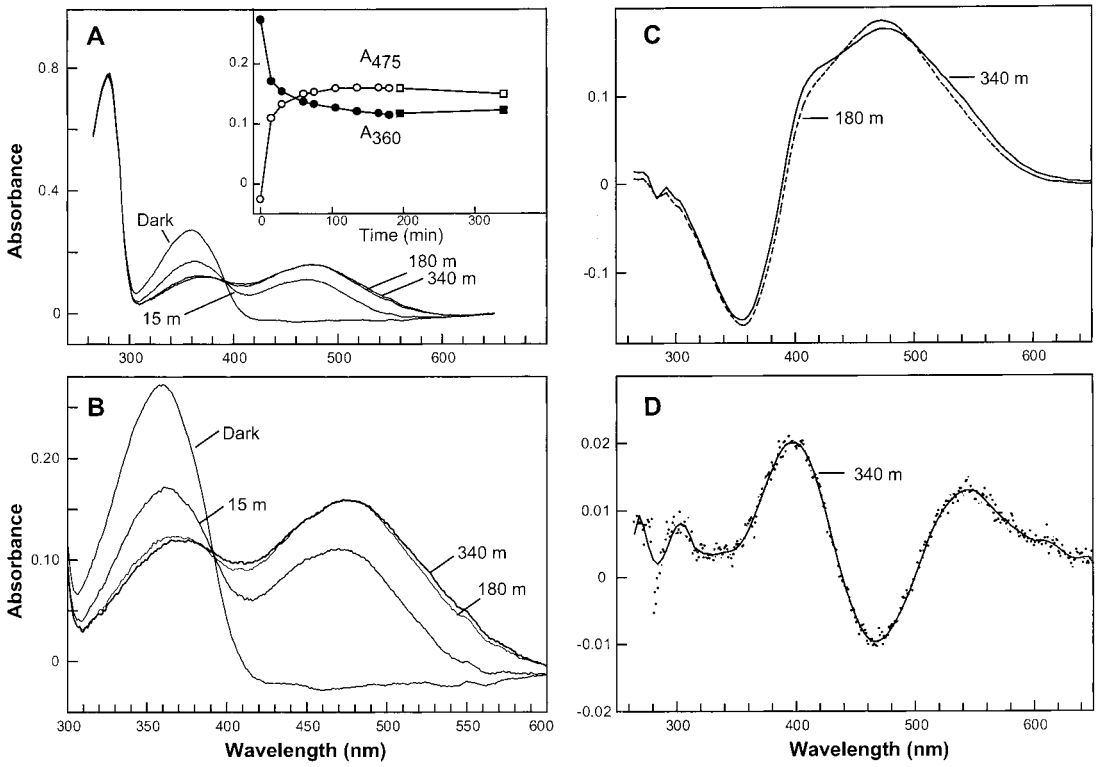


FIGURE 3: Photochemistry of the mouse SWS1 at 243 K. The mouse SWS1 (dark) was illuminated at 243 K with 305 nm light successively. (A and B) Spectra of the dark state and after 60, 120, 240, and 340 min of illumination. The inset in (A) shows a plot of the absorbance changes monitored at 360 and 475 nm during the illumination procedure. (C) Light − dark difference spectra obtained by subtracting the dark state from the PSS305 after 180 and 340 min of illumination at 243 K. (D) Difference spectrum of the PSS305 after 340 min of illumination and the PSS305 after 180 min of illumination. The red shift in the PSS305 is apparent at this temperature. The line is a smoothed fit (third-order polynomial regression, SigmaPlot, Jandel Scientific) to the difference spectrum.

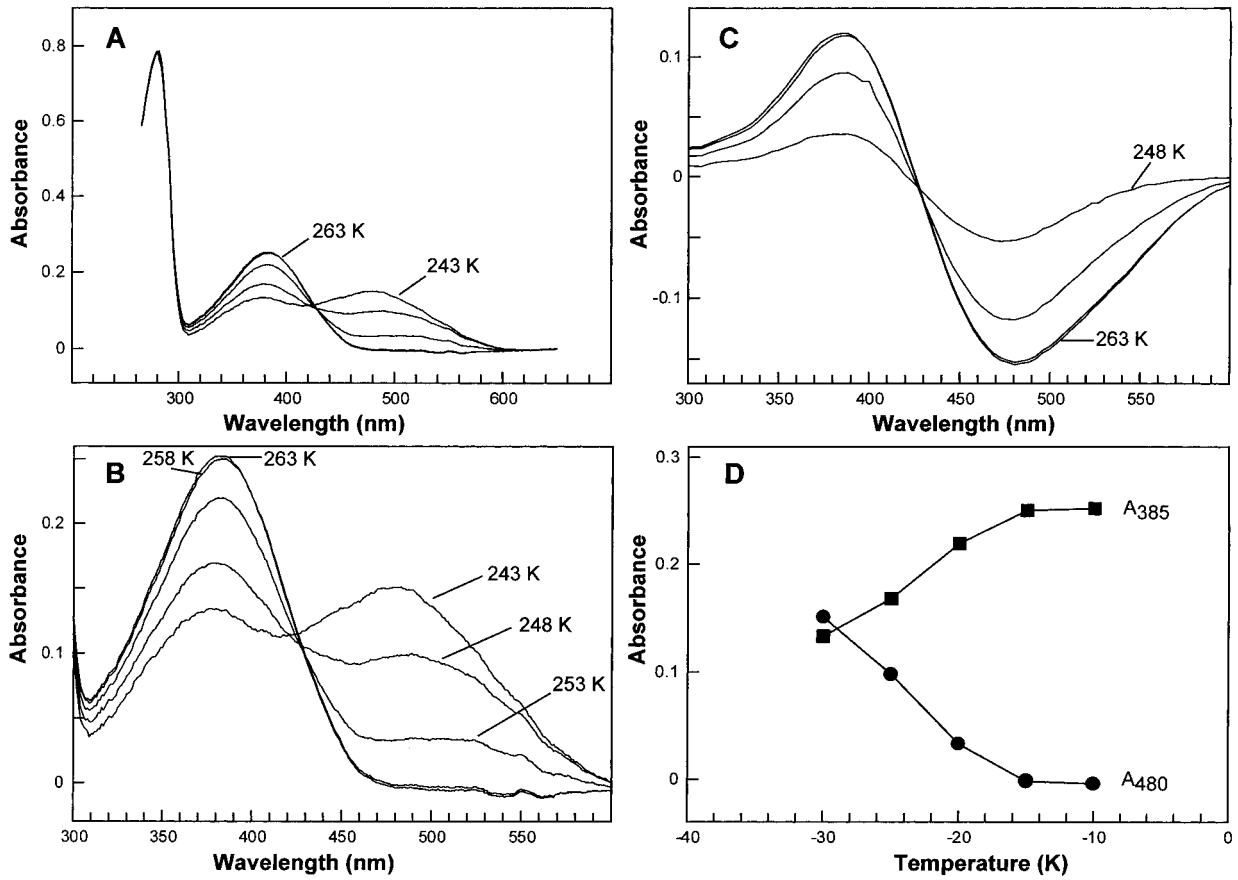


FIGURE 4: Thermal decay of the mouse SWS1 photostationary state formed at 243 K. The PSS305 formed at 243 K was gradually increased in 5 K increments. (A and B) Spectra of the PSS305 at 243 K and states formed after equilibration at 248, 253, 258, and 263 K. (C) Difference spectra between the PSS305 at various temperatures and the initial PSS305 formed at 243 K. (D) Plot of the absorbance changes monitored at 385 and 480 nm during the warming experiments.

spectrum. The presence of such an intermediate was also suggested during deconvolution of the spectra (see Discussion). The increase in absorbance with $\lambda_{max}$ ~440 nm strongly suggests that the MUV *lumi* intermediate has a protonated Schiff base linkage like other visual pigments. The protein absorbance recovers to that of the dark state, suggesting that conformational strains that were induced in the formation of *batho* are relaxed during the formation of *lumi*.

*Formation of the Later Intermediates.* To study the later photointermediates, we investigated the formation of the *meta I* and *meta II* states of MUV at temperatures >240 K, above the temperature required to form *lumi*. Illumination of the dark sample ($\lambda_{max}$ ~358 nm) at 305 nm, 243 K produced a photostationary state with a broad absorption band within 1 h (Figure 3A). However, after the initial decrease at 358 nm (within 1 h), no additional decrease at 358 nm was observed, even under extended illumination conditions (~6 h). Illumination of the sample produced a spectrum with a broad absorbance centered at ~470 nm and a decrease in the absorption at 358 nm (Figure 3A,B), which followed similar time courses (Figure 3A, inset). Prolonged illumination caused a further broadening of the red-shifted absorption band and a small reduction of the remaining dark state, with significant intensity beyond 600 nm (Figure 3C,D). The remaining absorbance at 358 nm was due to 11-*cis*-retinal bound to the protein, presumably arising from photoconversion of later intermediates back to the 11-*cis* form. Upon warming the illuminated sample, the absorption band at 358 nm progressively lost intensity while the band centered at 470 nm gained intensity with an isosbestic point at ~422 nm (Figure 4). Changes in the spectrum were essentially completed upon warming and equilibrating at 258 K. Despite repeated attempts, we were unable to acid-trap the protein−chromophore Schiff base linkage of the final species (data not shown). This is similar to the observation made with VCOP (*10*) and may represent an inherent property of all SWS1 pigments.

*Changes in MUV Protein Absorbance during the Formation of Photointermediates.* We observed a decrease in absorbance in the UV portion of the spectrum, 260−320 nm, upon the formation of PSS305 at 75 K (Figure 1). The drop in extinction was approximately 13%, which is equivalent to a $\Delta\epsilon$ of ~8500 $M^{-1}$ $cm^{-1}$ assuming an extinction coefficient at 280 nm of 65 000 $M^{-1}$ $cm^{-1}$ as for bovine rhodopsin.[2] The difference between PSS305 at 75 K and the dark spectrum was a broad peak centered around 290 nm, with bands at 281, 289, and 299 nm (Figure 5A). This drop in extinction recovered during the transition from *batho* to *lumi*, with the difference spectrum of PSS305 at 220 K and the dark spectrum exhibiting a number of small bands on the broad difference peak (Figure 5B). The protein absorbance changes that occurred in the transition from *meta I* to *meta II* were much smaller, with two distinct bands, at 293

[2] Estimated from $\epsilon^{500}$ = 40 600 $M^{-1}$ $cm^{-1}$ (*29*) and $A_{280}/A_{500}$ = 1.6 for purified rhodopsin (*30*). The aromatic amino acid composition of MUV (32 Phe/16 Tyr/7 Trp) is similar to bovine opsin (31 Phe/16 Tyr/5 Trp).

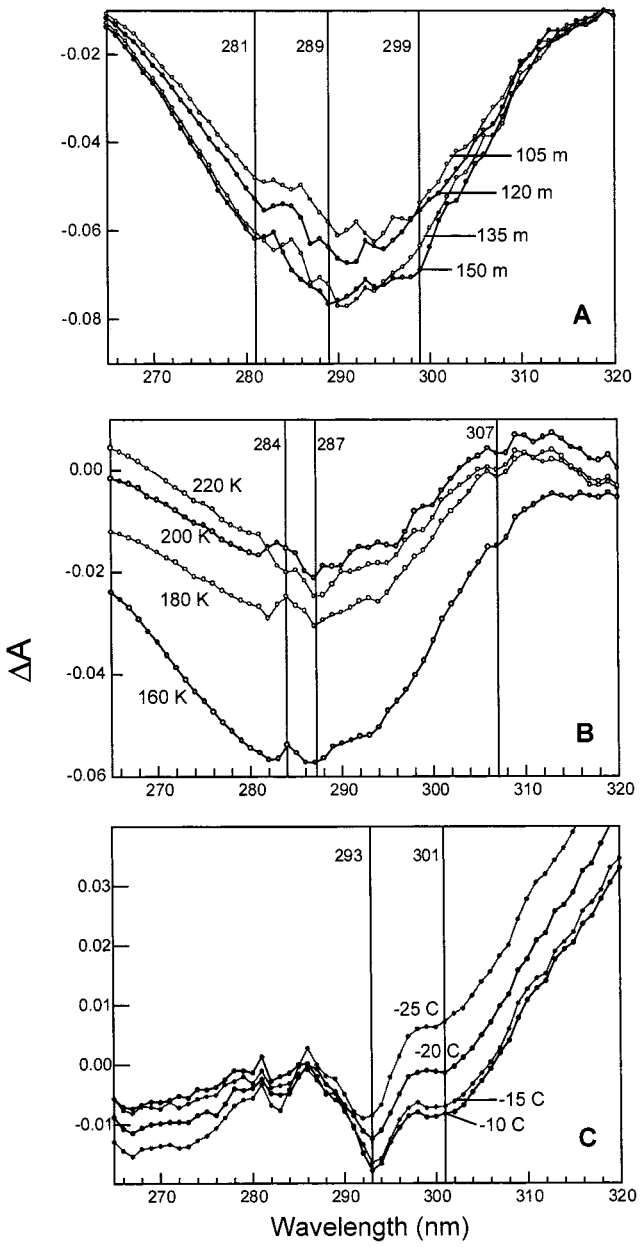


FIGURE 5: Photobleaching difference spectra of MUV between 260 and 320 nm. (A) Spectrum formed by illuminating MUV with 305 nm light at 75 K for the indicated duration (in minutes) was subtracted from the spectrum of the unilluminated sample. (B) Difference spectra were generated by subtracting the PSS305 spectra at the indicated temperatures from the dark spectrum at 75 K. (C) Difference spectra were generated by subtracting the PSS305 spectra at the indicated temperatures from the dark spectrum at −30 °C. Reference lines in each panel are given in nanometers.

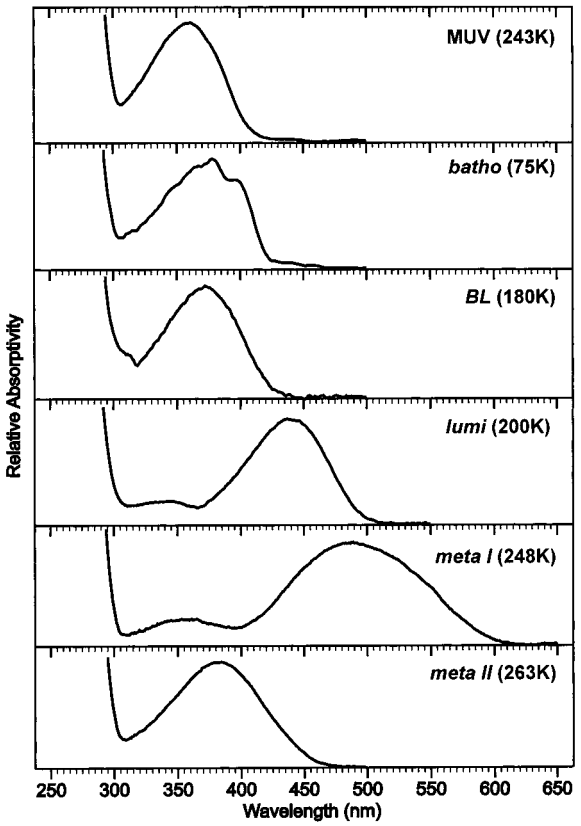


FIGURE 6: Calculated spectra of the photobleaching intermediates. Electronic absorption spectra of MUV and its photobleaching intermediates generated via decomposition of the temperature-trapped photostationary state spectra. Each spectrum is measured at the temperature indicated in the legend.

and 301 nm (Figure 5C). These changes are consistent with alterations in the environment of one or more of the aromatic residues, possibly tryptophan, since there are significant changes >290 nm.

*FTIR Spectroscopic Studies of the Protonation State of the Chromophore.* We carried out FTIR integral analysis of the 1100−1500 $cm^{-1}$ region of the *meta II* minus dark MUV vibrational spectrum using methodology outlined for the VCOP pigment (*10*). Our difference spectrum showed bands associated with the dark state of MUV at 1164, 1220, 1249, and 1270 $cm^{-1}$. A band at ∼1220 $cm^{-1}$ [see (*10*) for a discussion of this band, termed p2] is normally associated with a protonated chromophore. The integral value of the difference spectrum in the region between 1100 and 1500 $cm^{-1}$ of this band was compared to theoretical simulations (Table 1). It is clear from this analysis that the intensity of this region in the MUV is greatly reduced compared to rhodopsin and VCOP, and similar to the integral found in the bovine rhodopsin E113Q mutant, which has an unprotonated Schiff base at pH 6.8 (*31*). We conclude that the chromophore in the 11-*cis* dark state of MUV is unprotonated. The theoretical simulations of the MUV binding site (Figure 8) using mixed density functional and semiempirical methods theoretically predict a 1227 $cm^{-1}$ band that includes a mixing of the chromophore modes with nearby protonated glutamic acid modes. This provides an explanation for the observed intensity of the 1220 $cm^{-1}$ band.

*Derivation of the Spectra of MUV Intermediates.* Spectra of the pure intermediates were calculated by deconvolution using the HPLC results to assign the isomeric composition of PSS305 and assuming that the amount of the dark (11-cis) and light (11-*cis*, all-*trans*, and 9-*cis*) states remained constant during the temperature experiments described above (Figure 6). In contrast to other visual pigments, the *lumi* and *meta I* intermediates are significantly red-shifted compared to the *batho* intermediate. The $\lambda_{max}$ of the *lumi* ($\lambda_{max}$ ∼440 nm) intermediate of MUV is the same as that of protonated Schiff base model compounds in solution, thus indicating that the Schiff base in the MUV pigment undergoes a protonation during photobleaching. The blue shift of the $\lambda_{max}$ to 385 nm upon formation of *meta II* indicates that the formation of this intermediate is accompanied by the

Table 1: Comparison of Observed and Calculated Integrals for the *meta II* Minus Dark FTIR Difference Spectra[a]

| Experimental Measurements | | | |
|---|---|---|---|
| protein | pH | Schiff base | integral value |
| solubilized rhodopsin | 6.8 | protonated | −0.149 ± 0.037 |
| E113Q rhodopsin | 8.2 | unprotonated | −0.034 ± 0.042 |
| VCOP | 6.8 | protonated | −0.146 ± 0.051 |
| mouse UV (MUV) | 6.8 | (see Discussion) | −0.041 ± 0.048 |

| Theoretical Simulations | | | |
|---|---|---|---|
| 11-cis chromophore | method[b] | p2 band (int.)[c] | integral value |
| MUV binding site[d] (SB) | B3LYP, 6-31G | 1227.3 (216) | −0.072 |
| MUV binding site[d] (PSB) | B3LYP, 6-31G | 1230.2 (424) | −1.461 |
| unprotonated Schiff base (SB) | B3LYP, 6-31G | 1221.1 (55.5) | −0.014 |
| SB | B3LYP, 6-31G(d) | 1203.8 (63.2) | 0.006 |
| protonated Schiff base (PSB) | B3LYP, 6-31G | 1247.2 (1579.5) | −0.816 |
| PSB + perchlorate | B3LYP, 6-31G | 1233.6 (413.9) | −0.262 |
| PSB + perchlorate + 2 waters | HF, 6-31G(d) | 1218.9 (443.0) | −0.180 |

[a] All the experimental integral values are for *meta II* minus dark state and were measured from 1100 to 1500 $cm^{-1}$ in units of $cm^{-1}$ with the values normalized by adjusting the amide I band absorptivity to 1. The theoretical values are calculated relative to the all-trans unprotonated Schiff base (e.g., *meta II*-like) chromophore (B3LYP, 6-31G) with the integrals normalized to the central amide I band of polyglycine multiplied by the total number of residues in the protein [see ref (*10*)]. [b] Calculations were carried out using *Gaussian 98* (*51*). [c] Location in wavenumber of the intense mode, labeled p2 in the isolated protonated Schiff base, which corresponds to the observed mode at ∼1238 $cm^{-1}$ in rhodopsin and, by analogy, at 1232 $cm^{-1}$ in VCOP [see ref (*10*)]. The intensity is in KM/mol. [d] The calculations were carried out using the ONIUM method with a semiempirical basis set for the surrounding binding site (PM3) and density functional methods (B3LYP, 6-31G) to handle the chromophore, the water molecule near the Schiff base, and the nearby E108 counterion.

deprotonation of the Schiff base, as observed in other visual pigments (*28*).

## DISCUSSION

The photobleaching pathway of the MUV opsin is schematically represented in Figure 7. Upon illumination at 75 K, MUV forms a *batho* state, $\lambda_{max}$ ∼375 nm, with significant fine structure, as expected for an unprotonated Schiff base (*32*). In our previous study of MUV (*3*), we compared the difference spectra of the bathochromic photoproduct photostationary state with other visual pigments and found that MUV did not fit the trend that the other visual pigments followed, i.e., a linear correlation of the PSS-integrated spectrum with the $\lambda_{max}$ of PSS difference spectra [see (*3*) for discussion]. However, due to the lower protein concentration in that study, there was considerable light scattering in the absorbance spectra. The light scattering component was subtracted, and then all spectra were normalized at 280 nm for the analysis presented in (*3*). The light scattering obscured the changes in absorbance at ∼280 nm that occur during the formation of *batho* (Figures 1 and 5). With normalization, integration of the difference spectrum gave integral values of 2.1 and −1.9 (*3*). With the uncorrected absorbance (Figure 1), integral values are 1.89 and −1.36. These new values are well removed from the trend lines observed for the other pigments, and support the idea that the Schiff base is unprotonated in MUV.

At temperatures above 180 K, the MUV *batho* state starts forming a red-shifted *lumi* intermediate with a $\lambda_{max}$ ∼440 nm. Spectral deconvolution using previously described methods (*10*) indicates that another intermediate, slightly blue-shifted compared to *batho*, is formed during the *batho* to *lumi* transition. Henceforth, we refer to this intermediate as *BL* ($\lambda_{max}$ ∼370 nm), and is presumably analogous to the *BL* intermediate formed in the chicken blue opsin pathway (*33*). The formation of the *BL* intermediate is not obvious from the raw spectra during the temperature ramping experiments due to overlapping spectral features and fine structure (Figure 7).

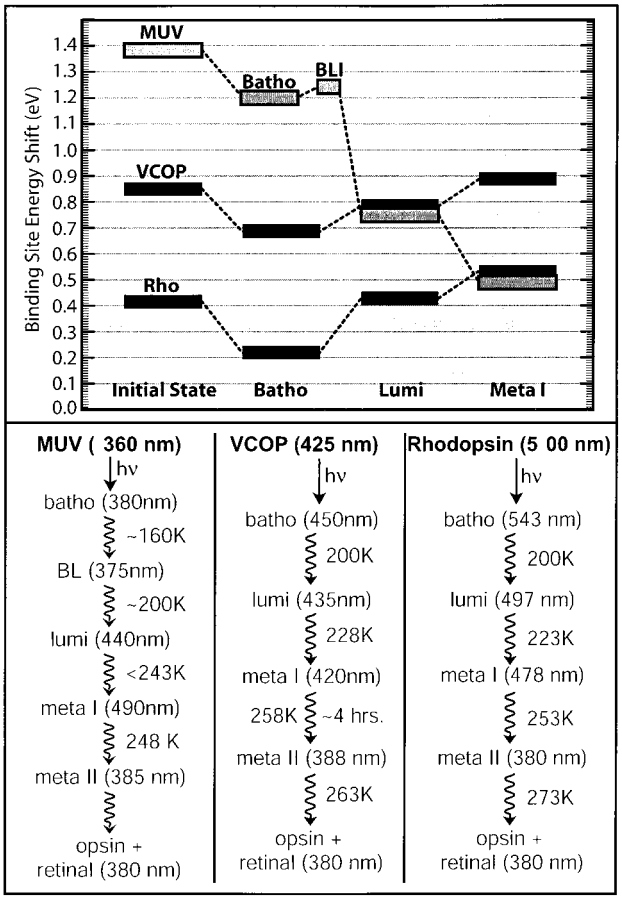


FIGURE 7: Photobleaching pathway of the mouse, *Xenopus* SWS1, and rhodopsin. The top portion of the figure shows the blue shift associated with incorporation of a hypothetical all-trans protonated Schiff base chromophore ($\lambda_{max}$ ∼600 nm) into the binding site for the protonated intermediates. The lower half shows a comparison of the photobleaching pathways of the mouse SWS1, the *Xenopus* SWS1, and rhodopsin. The *batho* intermediate ($\lambda_{max}$ ∼380 nm) is formed upon illumination at 75 K. *Batho* decays to *BL* ($\lambda_{max}$ ∼375 nm) at 160 K, which decays to *lumi* at 200 K. The lumi intermediate decays to meta I ($\lambda_{max}$ ∼490 nm) and then to meta II ($\lambda_{max}$ ∼385 nm) at 243 and 248 K, respectively.

The large spectral red shift coinciding with the formation of the MUV *lumi* intermediate raises two possibilities: the Schiff base remains unprotonated in the *batho* and *BL* intermediates and undergoes a protonation event during formation of the *lumi* intermediate. Alternatively, the Schiff base may undergo a protonation event during the formation of the *batho* intermediate, but have such a strained chromophore conformation that the $\lambda_{max}$ does not red shift to ~440 nm until the protein undergoes a large rearrangement during the transition to *lumi*, thus relieving the strain on the chromophore. Results from the photobleaching pathway of the MUV E108Q counterion mutant support the first alternative (in preparation).

The absorption maximum of the MUV *meta I* intermediate is very similar to that of the *meta I* intermediate formed in rhodopsin, although the MUV spectrum is much broader. This is surprising when compared to the VCOP *meta I* intermediate, which has an absorption maximum that is at 420 nm. Apart from the chicken blue opsin (*33*), MUV is the only opsin that has a *meta I* intermediate that is red-shifted compared to *lumi*. The MUV *meta I* intermediate decays to *meta II* at 248 K, and the transition is complete at 253 K (Figure 4B).

The three-dimensional structure of the MUV pigment has not yet been determined, but a homology model based upon the rhodopsin structure (*22*) reveals divergence between the retinal binding pocket of MUV and rhodopsin or VCOP (Figure 8). One striking difference is the putative location of F81, which is positioned very close to the Schiff base in the MUV binding site. This residue is highly conserved in other UV-sensitive pigments (e.g., salamander, zebrafish, *Anolis*) but varies in pigments that absorb above 400 nm, suggesting that F81 may play an important role in spectral tuning in the SWS1 pigments, possibly by regulating the p$K_a$ of the SB or by controlling the polarity of the SB environment. Another major variation in the predicted MUV retinal binding pocket is the absence of a highly conserved glutamic acid (E181 in bovine rhodopsin or E176 in VCOP) found in extracellular loop 2. This residue penetrates into the retinal binding pocket in the rhodopsin structure and contributes to the stability of *meta II* (*34*). In the MUV homology model, E176 is found to be interacting with the side chains of W186, Y187, and Y263 (not shown). However, since this residue is found in a loop region, our modeling results should be taken cautiously.

We investigated two possible molecular origins of the significant blue shift associated with the MUV pigment. The first mechanism we considered is deprotonation of the SB chromophore. Deprotonation will produce a chromophore that has a nominal absorption maximum between 355 and 380 nm based on experimental studies (*32*, *35*−*37*). The absorption maximum of MUV is in this range, and thus deprotonation provides the most straightforward source of the blue shift. Alternatively, two negatively charged counterions placed near the SB could affect theoretically a blue shift to 310 nm with a protonated SB (not shown). There are two potential counterions, E108 and E176, in the MUV. While our molecular dynamics calculations do not predict the necessary positioning of E176 (see discussion above), the calculations were carried out using harmonic constraints on the backbone, which may influence the predicted structure. However, the FTIR difference integral method presented and used in our previous assignment of the protonation state of the chromophore in the VCOP (*10*) supports the dark state of MUV being unprotonated.

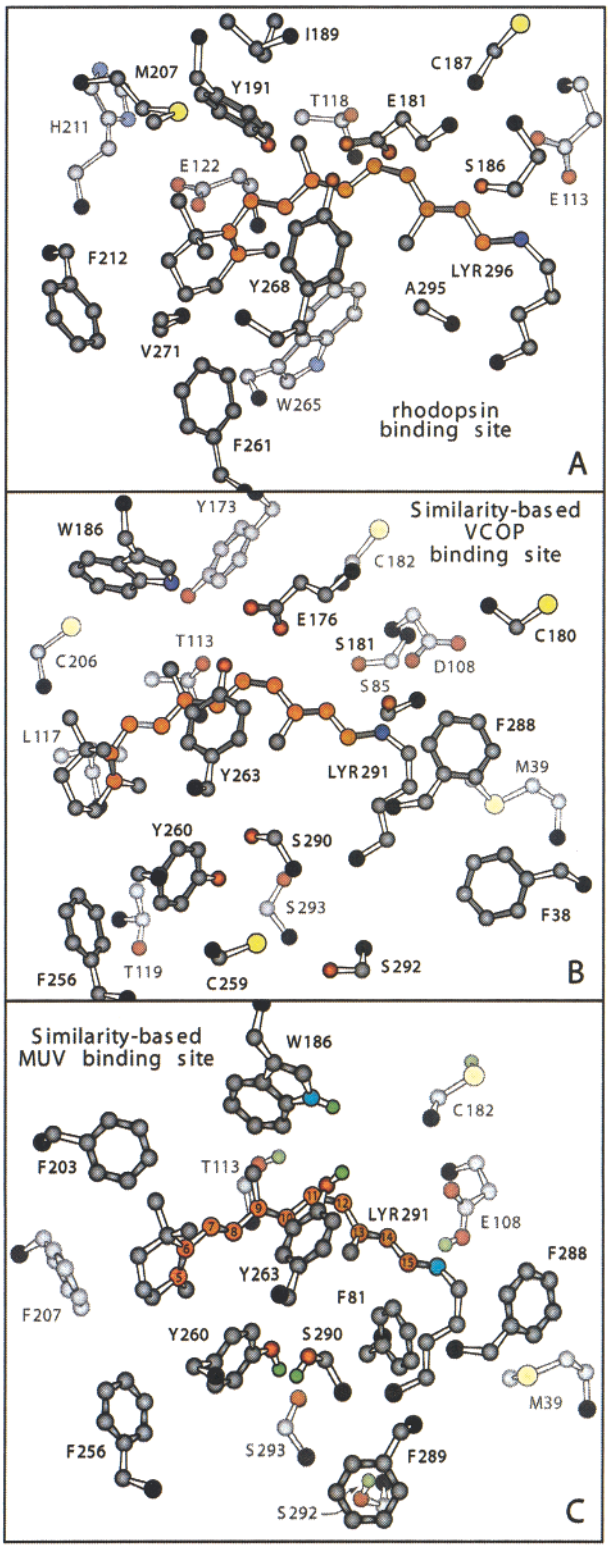


FIGURE 8: Homology models of the mouse and *Xenopus* SWS1 retinal binding sites compared to the rhodopsin retinal binding site. The rhodopsin binding site is taken from the crystal structure (*22*) and the VCOP model from our previous study (*10*). The MUV model was generated using analogous methods and procedures as discussed in the text. Residues that have their center of mass behind the plane of the chromophore are shown in lighter colors.

What determines the protonation state of SWS1 pigments? In the case of VCOP, the principal counterion is D108, and this counterion is stabilized via hydrogen bonding interactions with S85 (*4*). In MUV, D108 is replaced with E108, and this counterion would nominally be positioned closer to the chromophore. Density functional (B3LYP, 6-31G) molecular orbital simulations (not shown) indicate that when a glutamic acid counterion approaches to within ~3 Å of the SB proton, the SB hydrogen spontaneously migrates to the E108 residue, yielding an unprotonated chromophore. To have a protonated SB, either a relatively large stabilizing field within the binding site is necessary, which the calculations suggest does not exist in either MUV or VCOP, or the position of the counterion is stabilized by additional interactions, such as provided by S85 in VCOP (*4*). Both interactions appear to be absent in MUV.

In bovine rhodopsin, a number of structural changes occur in going from the dark to the *meta II* state, most notably the rigid-body motion of TM6 relative to the other helices and deprotonation of the Schiff base, leading to the active conformation (*38*). Deprotonation occurs during the transition from *meta I* to *meta II*, but it is not clear at what point in the photobleaching pathway the movement of TM6 occurs. Isomerization of the chromophore drives it into a highly strained all-trans conformation (*39*), with no large changes in protein conformation taking place during formation of the *batho* intermediate (*39, 40*). Photoaffinity cross-linking with retinal analogues has shown that the $\beta$-ionone ring interacts with W265 in TM6 in the dark and *batho* conformations, and interacts with A169 in TM4 in *lumi*, *meta I*, and *meta II* (*41*). The *batho* to *lumi* transition in bovine rhodopsin is also associated with changes in the protein backbone (*42*−*45*), although these changes have not been well characterized. UV absorbance spectroscopy (*46*−*48*), linear dichroism (*49*), and site-specific mutagenesis (*50*) have shown that the environments of two tryptophan residues, W126 and W265, are perturbed during the formation of the active state.

The results presented here show significant protein conformational changes in the formation of *batho* and *lumi* in MUV. These changes are directly reflected in the protein absorbance of aromatic residues, as well as the large change in the SB p$K_a$ upon formation of *lumi*, with apparent stoichiometric protonation. The formation of *meta II* also involves the deprotonation of the all-*trans*-retinal SB in *meta I*. Although the MUV and rhodopsin pigments have widely different absorbance properties in the dark, there appear to be conserved changes in both pigments following isomerization of the chromophore, including major protein conformational changes to form *lumi* with a protonated SB. The changes most likely involve the retinylidene SB environment, possibly alterations of the interactions with the counterion, E108, or F81, to permit electrostatic stabilization of the positive charge on the SB.

## NOTE ADDED IN PROOF

The importance of the F81 residue to spectral tuning in MUV and bovine blue has been recently demonstrated (*52*).

## REFERENCES


1. Ebrey, T., and Koutalos, Y. (2001) *Prog. Retinal Eye Res. 20*, 49−94.
2. Pitt, G. A., Collins, F. D., Morton, R. A., and Stok, P. (1955) *Biochem. J. 59*, 122−127.
3. Vought, B. W., Dukkipati, A., Max, M., Knox, B. E., and Birge, R. R. (1999) *Biochemistry 38*, 11287−11297.
4. Dukkipati, A., Vought, B. W., Birge, R. R., and Knox, B. E. (2001) *Biochemistry 40*, 15098−15108.
5. Starace, D. M., and Knox, B. E. (1997) *J. Biol. Chem. 272*, 1095−1100.
6. Fasick, J., Lee, N., and Oprian, D. (1999) *Biochemistry 38*, 11593−11596.
7. Ma, J. X., Kono, M., Xu, L., Das, J., Ryan, J. C., Hazard, E. S., Oprain, D. D., and Crouch, R. K. (2001) *Vis. Neurosci. 18*, 393−399.
8. Schneeweis, D. M., and Schnapf, J. L. (1999) *J. Neurosci. 19*, 1203−1216.
9. Perry, R., and McNaughton, P. (1991) *J. Physiol. 433*, 561−87.
10. Kusnetzow, A., Dukkipati, A., Babu, K. R., Singh, D., Vought, B. W., Knox, B. E., and Birge, R. R. (2001) *Biochemistry 40*, 7832−7844.
11. Babu, K. R., Dukkipati, A., Birge, R. R., and Knox, B. E. (2001) *Biochemistry 40*, 13760−13766.
12. Yokoyama, S., Radlwimmer, F. B., and Kawamura, S. (1998) *FEBS Lett. 423*, 155−158.
13. Shi, Y., Radlwimmer, F. B., and Yokoyama, S. (2001) *Proc. Natl. Acad. Sci. U.S.A. 98*, 11731−11736.
14. Sakmar, T. P., Franke, R. R., and Khorana, H. G. (1989) *Proc. Natl. Acad. Sci. U.S.A. 86*, 8309−8313.
15. Nathans, J. (1990) *Biochemistry 29*, 9746−9752.
16. Zhukovsky, E. A., and Oprian, D. D. (1989) *Science 246*, 928−931.
17. Doukas, A. G., Aton, B., Callender, H., and Ebrey, T. G. (1978) *Biochemistry 17*, 2430−2435.
18. Longstaff, C., Seckler, B., Calhoon, R. D., and Rando, R. R. (1987) in *Biophysical studies of retinal proteins* (Ebrey, T. G., Frauenfelder, H., Honig, B., and Nakanishi, K., Eds.) pp 64−70, University of Illinois Press, Champaign, IL.
19. Weitz, C. J., and Nathans, J. (1993) *Biochemistry 32*, 14176−14182.
20. Rao, V. R., Cohen, G. B., and Oprian, D. D. (1994) *Nature 367*, 639−642.
21. Lewis, J., Szundi, I., Fu, W., Sakmar, T., and Kliger, D. (2000) *Biochemistry 39*, 599−606.
22. Palczewski, K., Kumasaka, T., Hori, T., Behnke, C. A., Motoshima, H., Fox, B. A., Le Trong, I., Teller, D. C., Okada, T., Stenkamp, R. E., Yamamoto, M., and Miyano, M. (2000) *Science 289*, 739−745.
23. Thompson, J. D., Higgins, D. G., and Gibson, T. J. (1994) *Nucleic Acids Res. 22*, 4673−4680.
24. Vriend, G. (1990) *J. Mol. Graph. 8*, 52−56.
25. Brooks, B., Bruccoleri, R. E., Olafson, B. D., States, D. J., Swaminathan, S., and Karplus, M. (1983) *J. Comput. Chem. 4*, 187−217.
26. MacKerell, A. D., Jr., Bashford, D., Bellott, M., Dunbrack, R. L., Evanseck, J. D., Field, M. J., Fischer, S., Gao, J., Guo, H., Ha, S., Joseph-McCarthy, D., Kuchnir, L., Kuczera, K., Lau, F. T. K., Mattos, C., Michnick, S., Ngo, T., Nguyen, D. T., Prodhom, B., Reiher, W. E., III, Roux, B., Schlenkrich, M., Smith, J. C., Stote, R., Straub, J., Watanabe, M., Wiorkiewicz-Kuczera, J., Yin, D., and Karplus, M. (1998) *J. Phys. Chem. B 102*, 3586−3616.
27. Hermone, A., and Kuczera, K. (1998) *Biochemistry 37*, 2843−2853.
28. Shichida, Y., and Imai, H. (1998) *Cell Mol. Life Sci. 54*, 1299−315.
29. Wald, G., and Brown, P. K. (1953) *J. Gen. Physiol. 37*, 189−200.
30. Ridge, K. D., Lu, Z., Liu, X., and Khorana, H. G. (1995) *Biochemistry 34*, 3261−3267.
31. Sakmar, T. P. (1998) *Prog. Nucleic Acid Res. 59*, 1−34.
32. Murray, L. P., and Birge, R. R. (1985) *Can. J. Chem. 63*, 1967−1971.
33. Imai, H., Terakita, A., Tachibanaki, S., Imamoto, Y., Yoshizawa, T., and Shichida, Y. (1997) *Biochemistry 36*, 12773−12779.
34. Yan, E. C., Kazmi, M. A., De, S., Chang, B. S., Seibert, C., Marin, E. P., Mathies, R. A., and Sakmar, T. P. (2002) *Biochemistry 41*, 3620−3627.
35. Waddell, W. H., Schaffer, A. M., and Becker, R. S. (1977) *J. Am. Chem. Soc. 99*, 8456−8460.
36. Harosi, F. I., Favrot, J., Leclercq, Vocelle, D., and Sandorfy, C. (1978) *Rev. Can. Biol. 37*, 257−271.
37. Sandorfy, C., Lussier, L. S., Thanh, H. L., and Vocelle, D. (1987) in *Biophysical studies of retinal proteins* (Ebrey, T. G., Frauen-

felder, H., Honig, B., and Nakanishi, K., Eds.) pp 247−251, University of Illinois Press, Champaign, IL.
38. Farrens, D. L., Altenbach, C., Yang, K., Hubbell, W. L., and Khorana, H. G. (1996) *Science 274*, 768−770.
39. Kandori, H., Shichida, Y., and Yoshizawa, T. (2001) *Biochemistry (Moscow) 66*, 1197−1209.
40. Kandori, H., and Maeda, A. (1995) *Biochemistry 34*, 14220−14229.
41. Borhan, B., Souto, M., Imai, H., Shichida, Y., and Nakanishi, K. (2000) *Science 288*, 2209−2212.
42. Ujj, L., Jager, F., and Atkinson, G. H. (1998) *Biophys. J. 74*, 1492−1501.
43. Ganter, U. M., Gärtner, W., and Siebert, F. (1988) *Biochemistry 27*, 7480−7488.
44. Maeda, A., Ohkita, Y. J., Sasaki, J., Shichida, Y., and Yoshizawa, T. (1993) *Biochemistry 32*, 12033−12038.
45. Imai, H., Mizukami, T., Imamoto, Y., and Shichida, Y. (1994) *Biochemistry 33*, 14351−14358.
46. Rafferty, C. (1979) *Photochem. Photobiol. 29*, 109−120.
47. Rafferty, C., Mullenberg, C., and Shichi, H. (1980) *Biochemistry 19*, 2145−2151.
48. Lewis, J., Jager, S., and Kliger, D. (1997) *Photochem. Photobiol. 66*, 741−746.
49. Chabre, M., and Breton, J. (1979) *Photochem. Photobiol. 30*, 295−299.
50. Lin, S. W., and Sakmar, T. P. (1996) *Biochemistry 35*, 11149−11159.
51. Frisch, M. J., Trucks, G. W., Schlegel, H. B., Scuseria, G. E., Robb, M. A., Cheeseman, J. R., Zakrzewski, V. G., Montgomery, J. A., Stratmann, R. E., Burant, J. C., Dapprich, S., Millam, J. M., Daniels, A. D., Kudin, K. N., Strain, M. C., Farkas, O., Tomasi, J., Barone, V., Cossi, M., Cammi, R., Mennucci, B., Pomelli, C., Adamo, C., Clifford, S., Ochterski, J., Petersson, G. A., Ayala, P. Y., Cui, Q., Morokuma, K., Malick, D. K., Rabuck, A. D., Raghavachari, K., Foresman, J. B., Cioslowski, J., Ortiz, J. V., Stefanov, B. B., Liu, G., Liashenko, A., Piskorz, P., Komaromi, I., Gomperts, R., Martin, R. L., Fox, D. J., Keith, T., Al-Laham, M. A., Peng, C. Y., Nanayakkara, A., Gonzalez, C., Challacombe, M., Gill, P. M. W., Johnson, B. G., Chen, W., Wong, M. W., Andres, J. L., Head-Gordon, M., Replogle, E. S., and Pople, J. A. (1998) Gaussian Inc., Pittsburgh, PA.
52. Fasick, J. I., Applebury, M. L., and Oprian, D. D. (2002) *Biochemistry 41*, 6860−6865.

BI025883G